Progress in Additive Manufacturing
https://doi.org/10.1007/s40964-025-01094-5

FULL RESEARCH ARTICLE

Energy absorption of 3D printed stochastic lattice structures under impact loading – design parameters, manufacturing, and testing

J. Cronau[1] · **F. Engstler**[1]

Received: 13 September 2024 / Accepted: 24 March 2025

Abstract
The Voronoi lattice structure is one of the stochastically distributed strut-based lattice structures. In contrast to non-stochastic lattice structures, this means that the geometric structure is based on a random distribution of struts based on the Voronoi algorithm. In distinction to conventional open-pore foams, which also have a stochastic distribution of pores, the additive manufacturing of such structures offers the advantage of being able to vary the design parameters locally. There are two main design parameters defining the density and thus potentially influencing the mechanical characteristics of this structure: the strut diameter and the density of the starting points of the Voronoi algorithm resulting in a density of struts. This quantifies the influence of these design parameters on the energy absorption capability of Voronoi structures. The structures are manufactured from polyamide 12 using the SLS process and are tested at impact speeds of 5 m/s showing promising potential for energy absorption applications. To furthermore improve these characteristics graded lattice structures are also investigated at which both the density of the structure and the diameter of the struts are varied. A Design of Experiments (DoE) approach was used to proof the results statistically. It was found that structures with a density of 25% have the highest specific energy absorption (SEA) value of the investigated specimens. In addition, the combination of a small strut diameter and a high number of struts should be selected for the application of energy absorption. Grading of the structures can not only reduce the first stress peak after impact but also decreases overall performance. In general, there is room for improvement in terms of energy absorption capabilities of these structures.

keyword Impact loading · Lattice structures · Voronoi · Energy absorption

1 Introduction

With the increasing popularity of 3D printing, the optimal utilization of process-specific freedoms is increasingly becoming the focus of research and development. One of these freedoms is the ability to produce almost infinitely complex components. One way of utilizing this advantage is the production of lattice structures, a type of metamaterial which was first mentioned by Deshpande, Ashby, and Evans in 2001 [1, 2].

Lattice structures are divided into two subgroups: stochastic and non-stochastic, also called periodic lattice structures. Stochastic lattice structures are randomly distributed structures, whereas non-stochastic structures describe periodic geometrically directed structures. They are then further subdivided into 2D, 3D, shell-based, and strut-based structures (Fig. 1) [2–4]. Lattice structures have a wide variety of properties and are therefore suitable for a wide range of applications. But precise knowledge of the properties of the individual structures, as well as the design of the various structures themselves, is necessary in order to develop products based on requirements and to integrate such structures into applications [3, 5, 6].

One of the properties of lattices structures that are particularly suited for is energy absorption. Therefore, there are already various studies in this field. Ashby et al. mentioned that the mechanical properties depend primarily on the relative density and topological configuration of the structure [5]. However, most lattice structures offer different approaches to adjusting the relative density: either the cell

✉ J. Cronau
julius.cronau@unibw.de

[1] Universität der Bundeswehr Munich,
Werner-Heisenberg-Weg 39, 85577 Munich, Germany

Published online: 11 April 2025

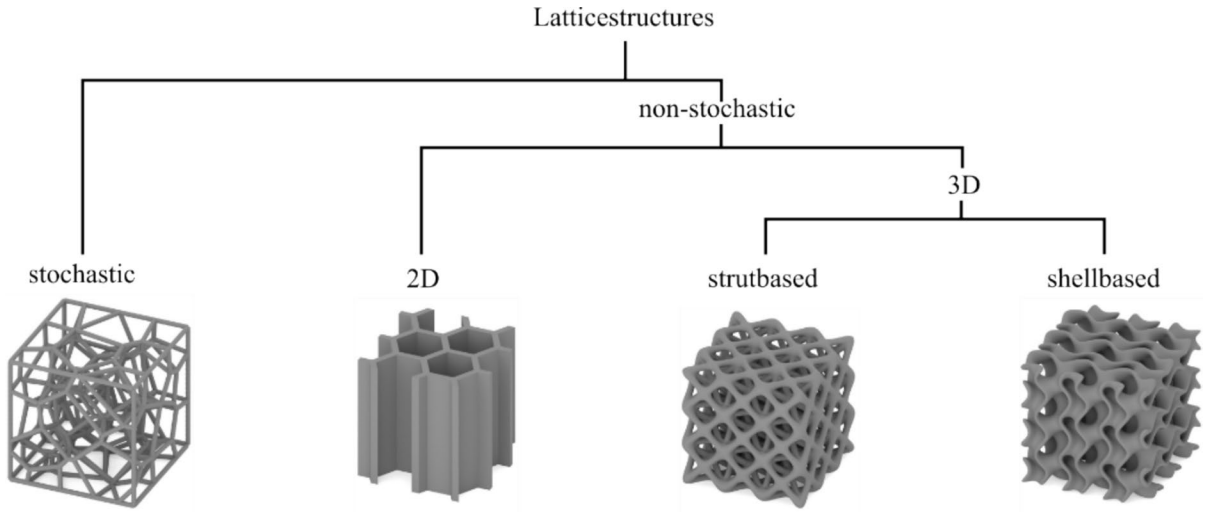

Fig. 1 Different types of lattice structures

size or the diameter/wall thickness is varied. A lot of studies focus on the topological configuration of the structure which led to a lot of new and interesting structures, including bio inspired cell designs, triply periodic minimal surface (TPMS), mirrored cell arrays, and so called "meta grains" incorporated into the structures [7–11]. To further improve the mechanical capabilities, grading the structures has been investigated and found to be a promising approach in some instances [12–15].

Most of the literature is testing the structures in a uniaxial compression test to determine the energy absorption capabilities. Many interesting applications, however, desire faster strain rates, such as helmets or crash bumpers. It has been shown that it is important to examine the structures in a strain rate range that is expected in the application in order to get comparable data. Polymers in particular often have strain rate-dependent material properties [16–18].

In addition, a precise knowledge of the influence of changes to the structure is necessary to bring these closer to the application. Bieler et al. not only investigated different design parameters at high strain rates for specimen made of thermoplastic polyurethane (TPU), which were produced using the stereolithography process (SLA), but also mentioned the process-specific geometric restrictions [19]. Maskery et al. showed that functionally graded shell-based lattice structures influence the elastic modulus significantly, while using material data of Selective Laser Sintered (SLS) Polyamid12 for his simulations [20]. Mueller et. al. did a computational study of periodic and stochastic lattice structures, using material data of Al-6101 T6, showing low peak stresses and high energy absorption capabilities of the stochastic lattice structures[21]. In summary, stochastic lattice structures show great potential for the application of energy absorption. Knowledge about the design of the individual parameters of the structures and the effect of grading is essential for the successful implementation of such structures in final products. The different 3d printing processes, materials, and strain rates must also be considered [16, 17].

One method to generate a stochastic lattice is through the Voronoi algorithm. The Voronoi algorithm, attributed to the mathematician Georgy Voronoi, is a pivotal method in computational geometry used to partition a space into distinct regions based on proximity to a predefined set of points. Each region, known as a Voronoi cell, encompasses all points that are closer to its corresponding seed point than to any other seed point. Mathematically, for a set of n seed points $\{p_1, p_2, \ldots, p_n\}$ in a Euclidean space, the Voronoi cell $V(p_i)$ for a seed p_i is defined as [22]

$$V(p_i) = \left\{ x \in \mathbb{R}^d \middle| \|x - p_i\| \leq \|x - pj\|, \forall j \neq i \right\} \quad (1)$$

Extending this concept to three-dimensional space enables the creation of complex 3D structures, which have significant applications in fields such as biology, material science, and computer graphics. Seed points in 3D Voronoi structures can be generated using various methods, including random distribution or based on specific criteria related to the application domain [22].

Groth et al. used a regular distributed set of points and added ellipsoids onto these points. Then a Gaussian distribution was used to create different randomization offsets for each ellipsoid. This method was used to influence randomness in every direction [23].

Ghouse et al. used a Poisson disk algorithm to fill a volume with randomly placed points [24].

A different approach is to use build in software tools, such as the pseudo-random point distribution of Grasshopper

plugin for Rhino software (Robert McNeel & Associates Inc) and influence the desired parameters afterward [25, 26].

Instead of using the Voronoi algorithm there are other methods to generate a lattice based on the stochastic distribution of points such as simply connecting each point with a specific set of rules. This leads to more parameters to influence the grid structure, the number of connections of each point, the minimum length of the connection, and the maximum length of the connection [21, 25, 26].

2 Materials and experimental procedures

2.1 Structure design

The specimen was designed using the software Rhino 8 with the plugin Grasshopper (Robert McNeel & Associates Inc). The random distribution tool which uses a random insertion algorithm was used to generate the base points for the Voronoi algorithm. The size of the samples was set at $30 \times 30 \times 30 mm^3$. To distribute the Voronoi cells more evenly and thus counteract random uneven distribution, the center of each Voronoi cell was determined and used as an input fort the next iteration of the Voronoi algorithm. This iterative procedure was repeated 5 times.

The struts were thickened using the Dendro (erc labs) plugin for Grasshopper. In order to determine the number of points that correspond exactly to the required relative densities various randomized correlations between density and points as well as the diameter were measured, and a function was created that describes this correlation. All tested specimens are shown in Fig. 2. In addition, the effect of the grading of the structures on the energy absorption capability was to be investigated. Therefore, two graded specimens were designed, one with graded diameter from 0.8 mm to 1.2 mm and one with graded bases points for the Voronoi algorithm. Despite the local differences in relative density, the overall relative density of the specimen is 20%. The graded specimen is also shown in Fig. 2.

2.2 Sample fabrication

The samples were produced using the SLS process. Two process-specific limitations are decisive for the design of the specimens. Firstly, the minimum feature size that can be produced is 0.7 mm on the EOS P396 (EOS GmbH, Krailling, Germany) SLS system used. The minimum diameter of the samples was therefore set at 0.8 mm. Secondly, after production in the SLS process the components are encased in a powder cake, which has a relatively high density. Therefore, there is a limitation regarding the depowdering of structures with a particularly high relative density. Despite treatment with compressed air and glass bead blasting, the powder inside the structures cannot be removed if the relative density of the samples exceeds a certain value. The maximum possible relative density also depends on the diameter of the structures. Figure 3 shows a sample of a graded structure to determine the maximum possible relative density with a diameter of 0.8 mm. The maximum relative density was therefore set at 25%.

The parameter set PA2200 Balance was used with a layer height of 120 µm. The build chamber temperature was set at 172 °C and the removal chamber temperature

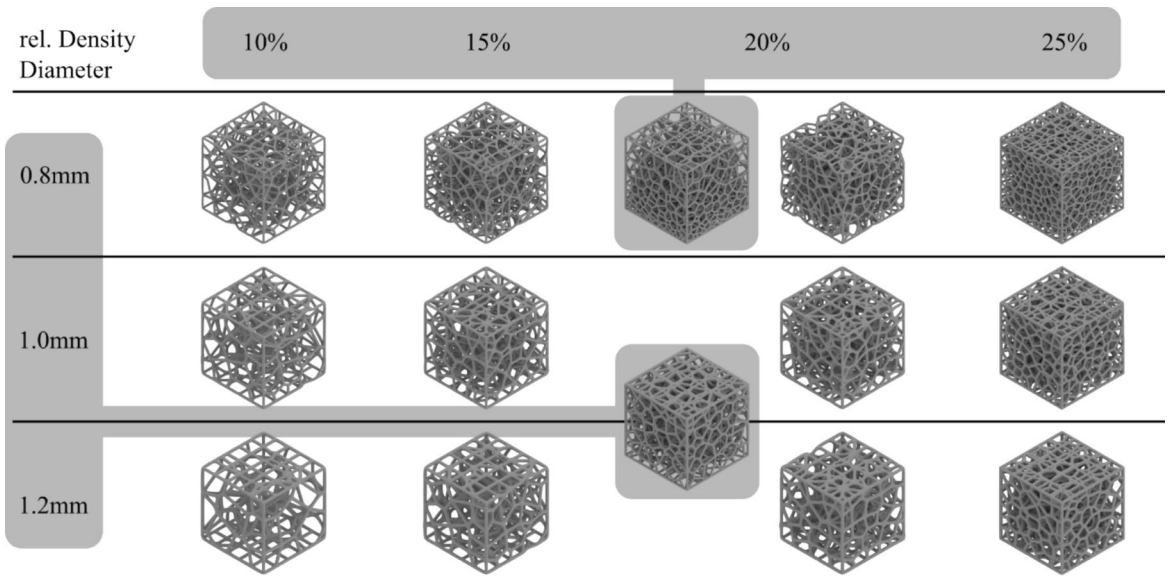

Fig. 2 Tested samples; the graded samples contain one grading of the points and one grading of the diameter over the examined range

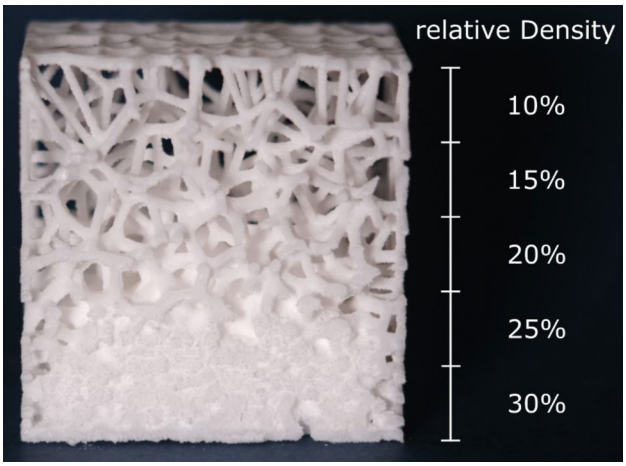

Fig. 3 Depowdering test sample, diameter 0.8 mm

at 130 °C. A blend of 50% used and 59% virgin PA12 powder was used to fabricate all specimen. All specimens were conditioned for at least one weak in standard climate (22 °C and 50% RH).

2.3 Testing methods

Since the use of the structure for impact scenarios is to be investigated here, a drop test is carried out. Many studies show that quasi-static tests cannot be attributed to the material behavior under high strain rates [17, 18]. The impacted speed is set at 5 m/s, which corresponds to the test speed of bicycle helmets, for example, DIN EN 1078 [27] being equivalent to a theoretical strain rate of 150^{-s} at the beginning of the experiment.

The drop tower test rig is a self-built unit, with a Kistler 9041 (Kistler Instrumente AG) force measuring device and a B&J type 4375 (Hottinger Brüel & Kjær A/S) acceleration sensor installed. The measured values are recorded by means of Kistler 5011 (Kistler Instrumente AG) charge measurement amplifiers and a LTT-186 (Labortechnik Tasler GmbH) transient recorder. The stress–strain curve is determined based on the force time data. To compare different structures and material in terms of energy absorption the specific energy absorption (SEA) per unit mass and the volumetric energy absorption (VEA) per volume are commonly used. To determine the energy absorption, the onset of densification is required. Comparison of different methods showed that the determination via the efficiency strain curve provides the best results [28]. Here, energy absorption is divided by the stress, whereby the densification point is located at the global maximum or at the last local maximum of the curve, depending on the structure [29, 30].

$$E(\sigma,\varepsilon)=\frac{\int_0^{\varepsilon}\sigma(\varepsilon)d\varepsilon}{\sigma(\varepsilon)}. \tag{2}$$

The VEA value is the area under the stress–strain curve up to the onset of densification ε_d.

$$VEA=\int_0^{\varepsilon_d}\sigma(\varepsilon)d\varepsilon. \tag{3}$$

Another common value is the total absorption efficiency of the structure. Here, the absorber under investigation is compared with an ideal absorber. The consideration here is that an ideal absorber maintains the maximum stress, which corresponds to the peak stress σ_p of the experiment before densification, from 0 to 100% strain.

$$E=\frac{\int_0^{\varepsilon_d}\sigma(\varepsilon)d\varepsilon}{\sigma_p}. \tag{4}$$

The SEA value is calculated from the VEA value divided by the density of the sample ρ_s, which must be determined for each sample due to the manufacturing deviations.

$$SEA=\frac{\int_0^{\varepsilon_d}\sigma(\varepsilon)d\varepsilon}{\rho_s}. \tag{5}$$

Another characteristic that is relevant for crash absorbers is the so-called force overshoot O. Here, the peak stress σ_p is divided by the plateau stress σ_{pl} so that a statement can be made about the evenness of the stress progression. If there are large differences between the peak stress and the plateau stress, this means uneven energy absorption and therefore high force peaks. The ideal absorber has a force overshoot of 1. The plateau stress is the average stress between the yield strain ε_y and the densification strain ε_d.

$$O=\frac{\sigma_p}{\sigma_{pl}} with\ \sigma_{pl}=\frac{\int_{\varepsilon_y}^{\varepsilon_d}\sigma(\varepsilon)d\varepsilon}{\varepsilon_d-\varepsilon_y}. \tag{6}$$

The results of these different performance parameters statistically monitored with the DoE software Modde Pro (Sartorius AG). The factors influencing the performance parameters were analyzed statistically at a significance level of 95%.

3 Results and discussion

3.1 Influence of design parameters

Both the SEA and the VEA values increase with increasing density of the specimen (Fig. 4). This means that the increase in weight and relative density improves the energy

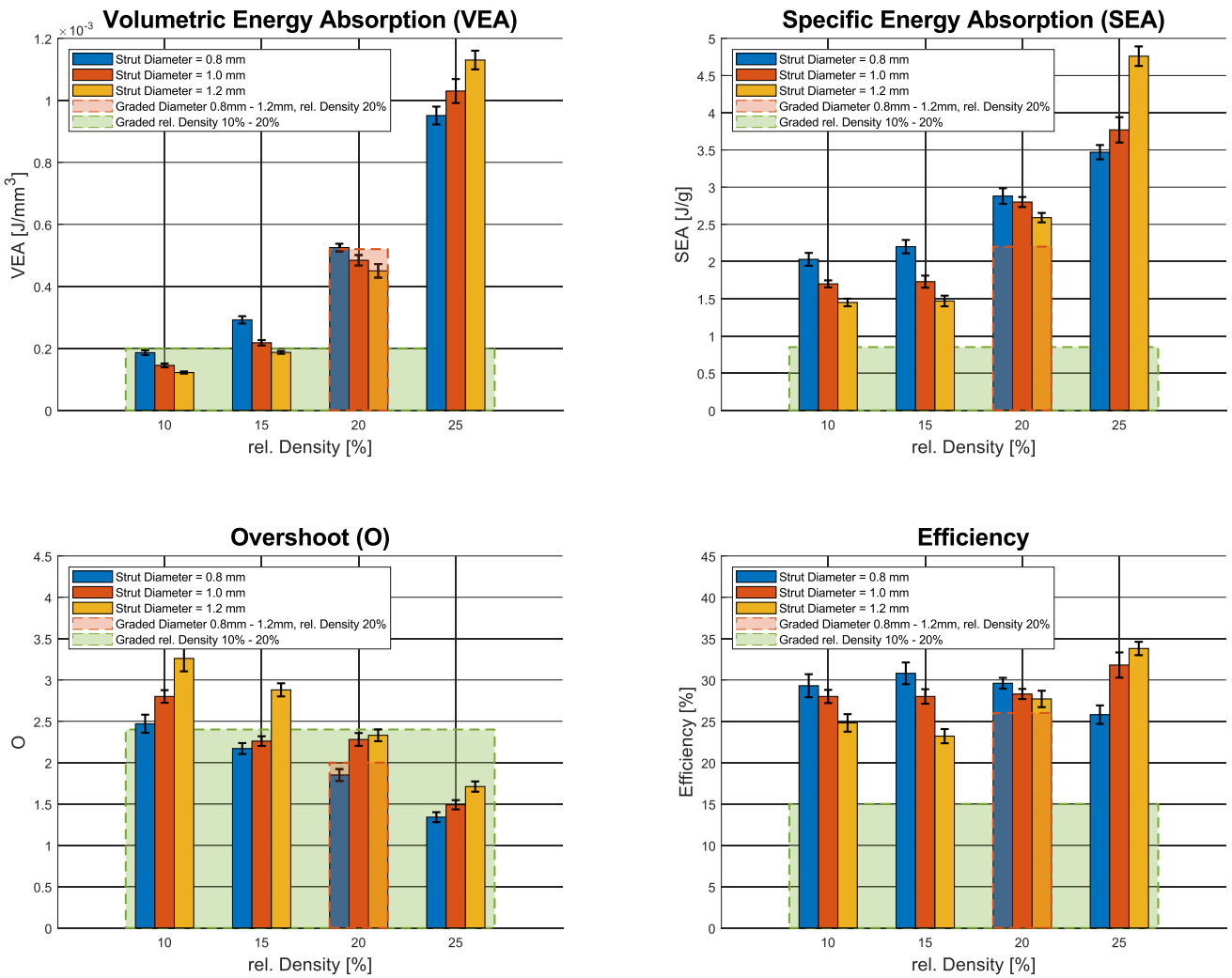

Fig. 4 Performance data of tested specimen. Relative density of graded specimen overall is 20%

absorption capacity disproportionately. The statistical analysis also shows that VEA and SEA are strongly influenced by the relative density within the framework of the factors under consideration. The variation of the diameter has a minimal influence on SEA and VEA at the above-mentioned level of significance (Fig. 5).

The stress–strain curves in Fig. 6 show that at lower relative densities of 10% and 15% the stress drops almost to 0 after the first peak, which indicates a brittle failure, which is also confirmed when looking at the high-speed video images (Fig. 7). For the specimens with a relative density of 10% (Fig. 7a, d), it is clear to see that fractures occur in many struts at the same time. It is also noticeable that the struts with a thinner diameter of 0.8 mm show greater deformation before fracture than those with 1.2 mm (Fig. 4a right top). By looking at the test of the higher-diameter (1.2 mm) specimen (Fig. 7 d,e,f) it can be deduced, that multiple fractures occur in one strut and the braking occurs often at the beginning or the end of the strut, and not so often in the middle of one strut.

The tests with a relative density of 25% and a diameter of 1.2 mm have the highest VEA and SEA values. The stress–strain curves show that the very strong drop in stress after the first force peak is not quite as strong in the specimens with a relative density of 25%. Especially the specimens with a diameter of 0.8 mm, on the other hand, show the lowest onset of densification, which can be explained by the high relative density (Fig. 4).

The overshoot data, which show the uniformity of the force curve, confirm this. The lowest overshoot is found in the samples of relative density of 25% and diameter of 0.8 mm and is just below 1.5, which means that the maximum stress reaches 1.5 times the plateau stress.

The statistical analysis shows that the overshoot is influenced by both factors, the diameter and the relative density. Lowering the diameter leads to a lower overshoot,

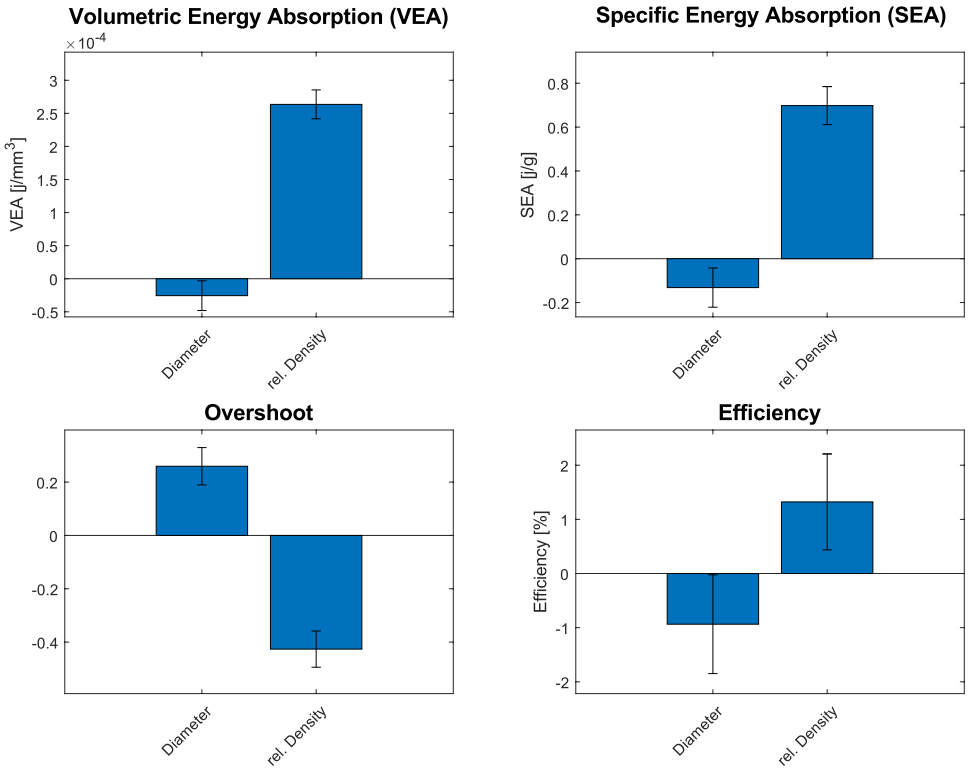

Fig. 5 Coefficient plot of examined factors showing the influence on the results as well as their interactions with a significance level of 95%. If the error bar crosses 0, there is no significant influence

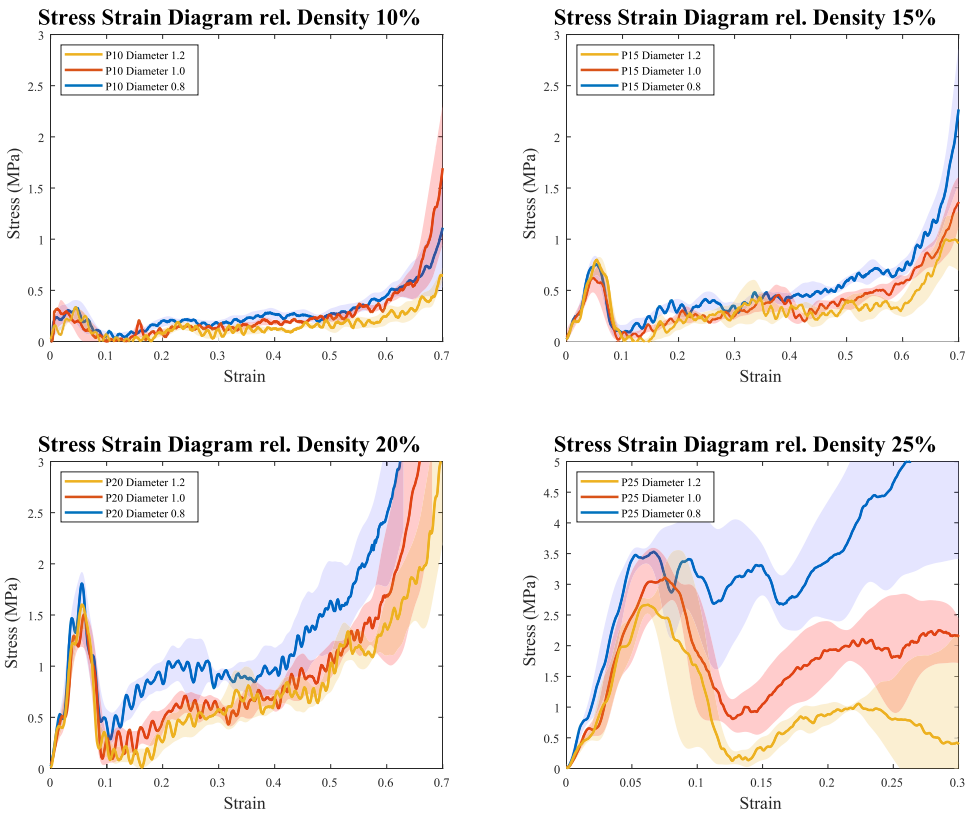

Fig. 6 Stress–strain diagram of different tested relative density levels and diameters

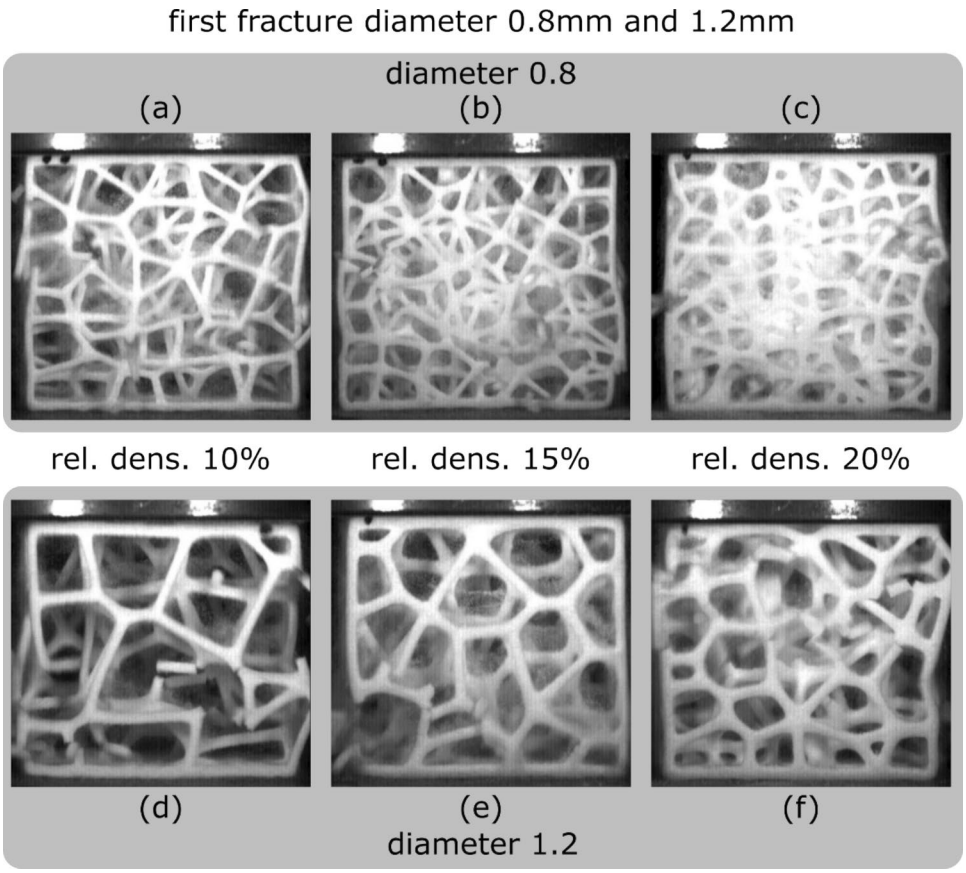

Fig. 7 High-speed camera pictures of the moment the first fracture occurs during drop tower testing

which seem logical, as the higher-diameter struts need more force to be broken. Also, a higher relative density leads to a lower overshoot. By looking at the video of the higher-diameter (1.2 mm) specimen (Fig. 7 d,e,f) it can be deduced that multiple fractures occur in one strut and the braking occurs often at the beginning or the end of the strut, and not so often in the middle of one strut.

Considering the total efficiency, the relative density has a minimal influence on the efficiency of the samples, while the diameter has no significant influence (Fig. 5). In general, the efficiency is between 20 and 35%, which is a low value compared to other crash absorbers or even other lattice structures made with polyamide 12 [24].

A look at the stress–strain curves (Fig. 6) shows that the low efficiency is due to the previously discussed sharp drop in stress after the first stress peak, i.e., after the first fracture. Ideally, the stress curve after the first force peak should remain at the highest possible stress level. In this case, however, the first fractures in the structure appear to occur over the entire area of the sample, after which the stress slowly builds up again.

In order to optimize the efficiency, the course of the curve would have to be optimized, which would also have positive effects on the performance characteristics. Above all, the sharp drop in stress after the start of the first fracture would have to be prevented. One idea would be to randomize the struts only locally, i.e., to randomly assign different diameters to the struts to prevent the breaking of an entire plane and thus the sharp drop in stress.

Another possibility would be to combine this structure with another lattice structure, which keeps the stress at a higher level after the fracture than is currently the case.

The only sample that shows a different behavior is a sample with a relative density of 25% and a diameter of 0.8 mm, where the stress does not drop as much (Fig. 6), which can also be seen in the low overshot value (Fig. 4), but a very early onset of densification occurs due to the high relative density. This behavior is not as pronounced for the samples with diameters of 1.0 mm and 1.2 mm and relative densities of 25%. Comparing the VEA value and the SEA value (Fig. 4) of the samples of relative density of 25% with 0.8 mm, 1.0 mm, and 1.2 mm diameters, the highest values correspond to the specimen with a diameter of 1.2 mm. However, the VEA values of the relative density of 25% differ less than the SEA values. It is possible that not all the powder could be removed from the very dense structures in post-processing. A problem that was already mentioned in a previous section on sample fabrication. Powder that is

still inside the structure leads to a higher weight of the sample and thus to a lower SEA value. The VEA value is not affected by this and the differences between the VEA values of the samples with a relative density of 25% are smaller than those between the SEA values (Fig. 4).

For the statistical analysis of the results, a quadratic D-optimal experimental design was fitted using the partial least squares (PLS) method [31]. The model shows good agreement with the experimental results, except for the efficiency response. As already discussed, the effects of the factors on efficiency are only minimal or not significant. The model is therefore not valid for the efficiency response. This is also shown by the R2 and Q2 values which represent the model fit and the estimated future prediction precision with 1 as a perfect value; the values of the present model are shown in Table 1. Figure 8 shows the normal probability of the residuals for SEA, VEA, and overshoot. All values lie in a range from -3 to 3, which means that the test data for this type of investigation is valid. If there were outliers in the dataset, they would fall out of this range.

Table 1 R2 and Q2 values for the fitted model

Response	R2	Q2
VEA	0.978	0.884
SEA	0.900	0.880
Efficiency	0.108	0.409
overshoot	0.863	0.796

Figure 9 shows a comparison of the model prediction and the measured parameters. The closer all points are to the line, the better the model represents the measured values. For SEA, VEA, and overshoot, there is good agreement, which has already been confirmed by the values shown in Table 1.

The prediction plots (Fig. 10) show a strong influence of the relative density on the responses, while the diameter, as discussed previously, only has a significant influence on the overshoot and a minimal influence on the SEA. As also discussed previously, with increasing relative density, the VEA and SEA increases, whereas the overshoot decreases. The prediction plots for the diameter were made with a set relative density of 17.5% and the plots for the relative density with a set diameter of 1.0, respectively.

Formulas 7, 8, and 9 show the model that represents the responses to the factors. For X_1 = diameter and X_2 = relative density the formulas with the respective coefficients were determined for the fitted, scaled, and centered model.

$$VEA = 0{,}000231989 - 1.72442e^{-5}X_1 + 0.000223434X_2 + 0.00013991{X_2}^2 + 2.1216e^{-5}X_1 * X_2, \tag{7}$$

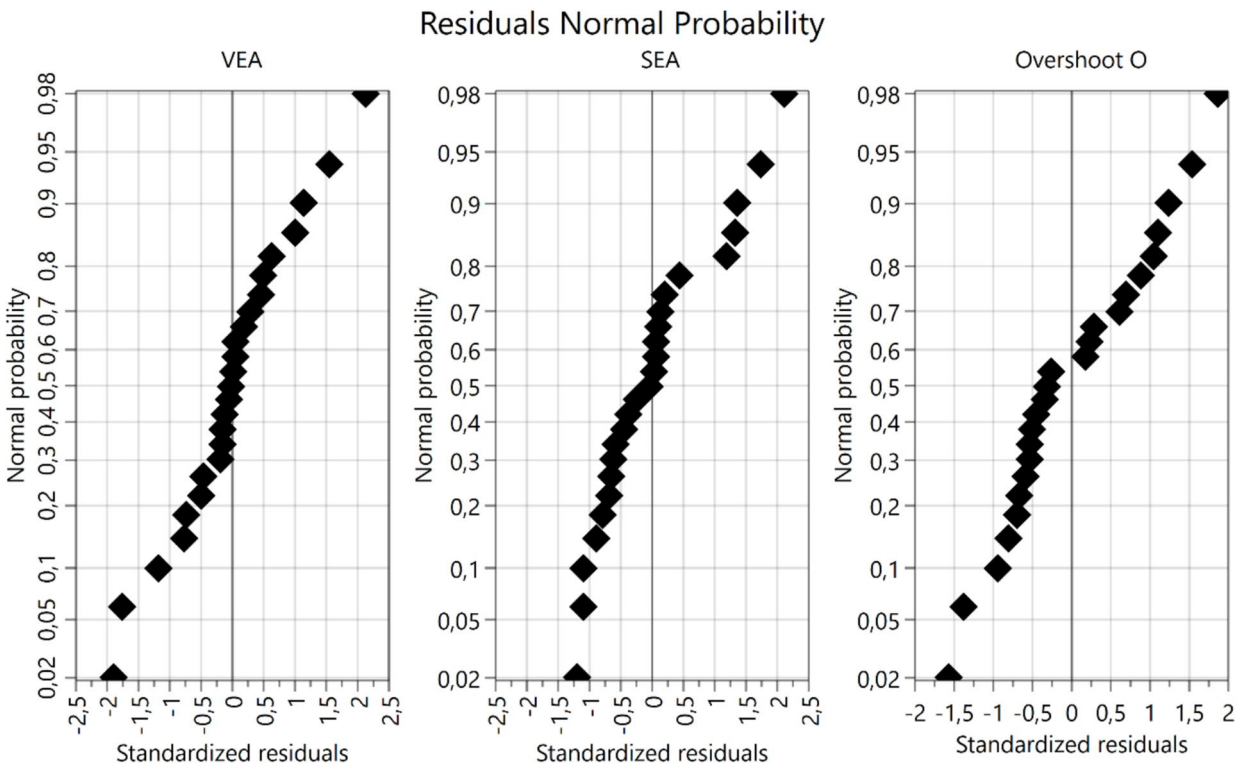

Fig. 8 Residuals normal probability for the tested data. All points between -3 and 3 indicate an acceptable dataset

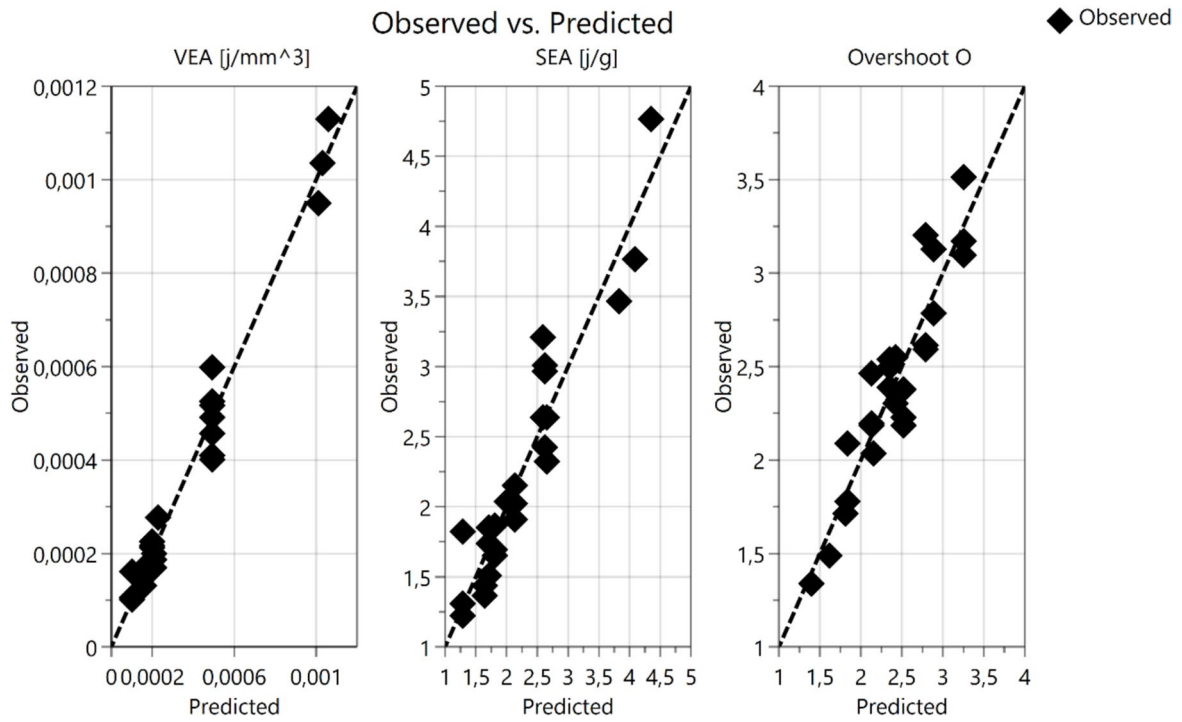

Fig. 9 Observed vs. predicted values for VEA, SEA, and overshoot

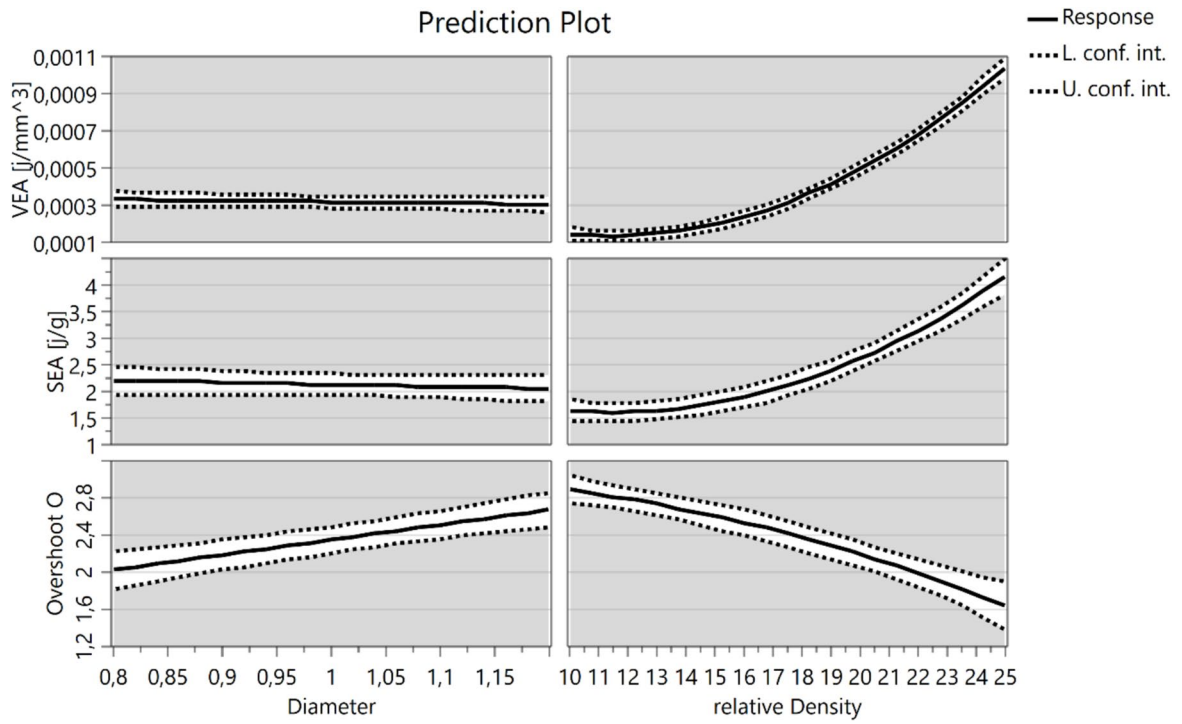

Fig. 10 Prediction plot of VEA, SEA, and overshoot O for both factors diameter and relative density with confidence bounds

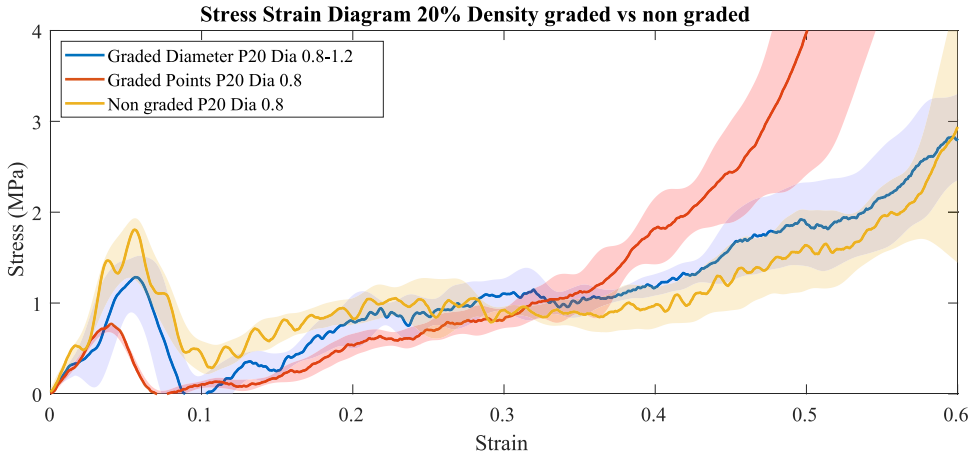

Fig. 11 Stress–strain diagram of graded specimen versus non-graded specimen with same diameter and relative density

$$SEA = 1.89589 - 0.12205X_1 + 0.604234X_2 + 0.392541{X_2}^2 + 0.192677X_1 * X_2, \tag{8}$$

$$O = 2.49047 + 0.279646X_1 - 0.37898X_2 - 0.0757602{X_2}^2 - 0.0679379X_1 * X_2. \tag{9}$$

3.2 Influence of grading

The graded specimens exhibit several effects in the drop tower test. On one hand, the grading of the specimens reduces the first stress peak (Fig. 11), which also has a positive effect on the overshot (Fig. 4). The first stress peak of the samples with grading in the points and a diameter of 0.8 mm is lower than that of the samples with graded diameters. On the other hand, the grading of the points in particular leads to a significantly earlier onset of densification strain (Fig. 11). While this sample has a very low density on one side, the effect occurs on the other side, which can already be observed in the samples with a generally high relative density. The very packed structure densifies even at low elongation. Figure 11 shows the stress–strain curves of the graded samples and the comparable sample with a relative density of 20% and a diameter of 0.8 mm. For the energy absorption, i.e., the SEA and VEA values, the grading of the samples does not bring any advantages. Rather, the grading of the structures leads to reduced energy absorption, a more pronounced stress drop after the first stress peak, and an early onset of densification strain.

4 Conclusion

In this study, Voronoi lattice structures made of polyamide 12 (PA2200) using the SLS process with a relative density of 10%–25% and a diameter of 0.8 mm to 1.2 mm were investigated. The results were analyzed statistically and a D-optimal model was fitted and showed good agreement with the test data. In general, the structures made of this material behave rather brittle at this strain rate. The first fracture of the structure was observed in all samples even before an elongation of 10%. The samples with the parameters relative density of 25% and a diameter of 1.2 mm showed the highest energy absorption in relation to volume (VEA) and weight (SEA). The reason for this is that the stress–strain curve is more uniform. Why exactly this curve, which differs greatly from the others, occurs could not be clarified exactly. Here, further investigations are necessary. The statistical analysis shows that the main factor influencing the increase in VEA and SEA values is relative density. A lower diameter generally favors a more uniform stress curve, with the exception of the so-called top performer with a relative density of 25% and a diameter of 1.2 mm. The grading of both the diameter and the density in the direction of force could reduce the first force peak, but the locally higher relative density causes an earlier onset of densification, which leads to reduced energy absorption. In general, the stress–strain curves, as well as the values of the overall efficiency, show potential to improve the energy absorption capacity. For this purpose, the strong stress drop after the first force peak would have to be minimized. One starting point could be to randomize the struts or to combine the Voronoi lattice structure with a structure that can compensate for this drop in stress.

Acknowledgements This research is funded by dtec.bw – Digitalization and Technology Research Center of the Bundeswehr. Dtec.bw is funded by the European Union – NextGenerationEU

Funding Open Access funding enabled and organized by Projekt DEAL.

Declarations

Conflict of interest On behalf of all authors, the corresponding author states that there is no conflict of interest.

References

1. Deshpande VS, Fleck NA, Ashby MF (2001) Effective properties of the octet-truss lattice material. J Mech Phys Solids 49:1747–1769. https://doi.org/10.1016/S0022-5096(01)00010-2
2. Evans AG, Hutchinson JW, Fleck NA et al (2001) The topological design of multifunctional cellular metals. Prog Mater Sci 46:309–327. https://doi.org/10.1016/S0079-6425(00)00016-5
3. Du Plessis A, Razavi SMJ, Benedetti M et al (2022) Properties and applications of additively manufactured metallic cellular materials: a review. Prog Mater Sci 125:100918. https://doi.org/10.1016/j.pmatsci.2021.100918
4. Tao W, Leu MC (2016) Design of lattice structure for additive manufacturing. In: 2016 International Symposium on Flexible Automation (ISFA). IEEE, [Place of publication not identified], pp 325–332
5. Ashby MF (2006) The properties of foams and lattices. Philos Transact A Math Phys Eng Sci 364:15–30. https://doi.org/10.1098/rsta.2005.1678
6. Dong G, Tessier D, Zhao YF (2019) Design of shoe soles using lattice structures fabricated by additive manufacturing. Proc Des Soc Int Conf Eng Des 1:719–728. https://doi.org/10.1017/dsi.2019.76
7. Chen X, Ren W, Sun Y et al (2022) Adjusting unit cell three-dimensional posture and mirror array: a novel lattice structure design approach. Mater Des 221:110852. https://doi.org/10.1016/j.matdes.2022.110852
8. Seek CY, Kok CK, Lim CH, Liew KW (2022) A novel lattice structure for enhanced crush energy absorption. Int J Technol 13:1139. https://doi.org/10.14716/ijtech.v13i5.5829
9. Wagner MA, Lumpe TS, Chen T, Shea K (2019) Programmable, active lattice structures: unifying stretch-dominated and bending-dominated topologies. Extreme Mech Lett 29:100461. https://doi.org/10.1016/j.eml.2019.100461
10. Mao A, Zhao N, Liang Y, Bai H (2021) Mechanically efficient cellular materials inspired by cuttlebone. Adv Mater Deerfield Beach Fla 33:2007348. https://doi.org/10.1002/adma.202007348
11. Liu C, Lertthanasarn J, Pham M-S (2021) The origin of the boundary strengthening in polycrystal-inspired architected materials. Nat Commun 12:4600. https://doi.org/10.1038/s41467-021-24886-z
12. Al-Ketan O, Lee D-W, Rowshan R, Abu Al-Rub RK (2020) Functionally graded and multi-morphology sheet TPMS lattices: design, manufacturing, and mechanical properties. J Mech Behav Biomed Mater 102:103520. https://doi.org/10.1016/j.jmbbm.2019.103520
13. Al-Saedi DSJ, Masood SH, Faizan-Ur-Rab M et al (2018) Mechanical properties and energy absorption capability of functionally graded F2BCC lattice fabricated by SLM. Mater Des 144:32–44. https://doi.org/10.1016/j.matdes.2018.01.059
14. Maskery I, Hussey A, Panesar A et al (2017) An investigation into reinforced and functionally graded lattice structures. J Cell Plast 53:151–165. https://doi.org/10.1177/0021955X16639035
15. Wen Z, Li M (2021) Compressive properties of functionally graded bionic bamboo lattice structures fabricated by FDM. Mater Basel Switz. https://doi.org/10.3390/ma14164410
16. Zhang J, Lu G, You Z (2020) Large deformation and energy absorption of additively manufactured auxetic materials and structures: a review. Compos Part B Eng 201:108340. https://doi.org/10.1016/j.compositesb.2020.108340
17. Mirhakimi A, sadat, Dubey D, Elbestawi MA, (2024) Laser powder bed fusion of bio-inspired metamaterials for energy absorption applications: a review. J Mater Res Technol 31:2126–2155. https://doi.org/10.1016/j.jmrt.2024.06.234
18. Yin H, Zhang W, Zhu L et al (2023) Review on lattice structures for energy absorption properties. Compos Struct 304:116397. https://doi.org/10.1016/j.compstruct.2022.116397
19. Bieler S, Weinberg K (2024) Energy absorption of sustainable lattice structures under impact loading. arXiv. arxiv.org/abs/2412.06547
20. Maskery I, Aremu AO, Parry L et al (2018) Effective design and simulation of surface-based lattice structures featuring volume fraction and cell type grading. Mater Des 155:220–232. https://doi.org/10.1016/j.matdes.2018.05.058
21. Mueller J, Matlack KH, Shea K, Daraio C (2019) Energy absorption properties of periodic and stochastic 3D lattice materials. Adv Theory Simul 2:1900081. https://doi.org/10.1002/adts.201900081
22. Syta H, Weygaert R (2009) Life and Times of Georgy Voronoi. arXiv. https://doi.org/10.48550/arXiv.0912.3269
23. Groth J-H, Anderson C, Magnini M et al (2022) Five simple tools for stochastic lattice creation. Addit Manuf 49:102488. https://doi.org/10.1016/j.addma.2021.102488
24. Ghouse S, Babu S, Nai K et al (2018) The influence of laser parameters, scanning strategies and material on the fatigue strength of a stochastic porous structure. Addit Manuf 22:290–301. https://doi.org/10.1016/j.addma.2018.05.024
25. Hossain U, Ghouse S, Nai K, Jeffers JR (2021) Controlling and testing anisotropy in additively manufactured stochastic structures. Addit Manuf 39:101849. https://doi.org/10.1016/j.addma.2021.101849
26. Kechagias S, Oosterbeek RN, Munford MJ et al (2022) Controlling the mechanical behaviour of stochastic lattice structures: the key role of nodal connectivity. Addit Manuf 54:102730. https://doi.org/10.1016/j.addma.2022.102730
27. (2014) DIN EN 1078:2014–04, Helme für Radfahrer und für Benutzer von Skateboards und Rollschuhen; Deutsche Fassung EN_1078:2012+A1:2012. Beuth Verlag GmbH, Berlin
28. Li QM, Magkiriadis I, Harrigan JJ (2006) Compressive strain at the onset of densification of cellular solids. J Cell Plast 42:371–392. https://doi.org/10.1177/0021955X06063519
29. Niu X, Xu F, Zou Z et al (2022) In-plane dynamic crashing behavior and energy absorption of novel bionic honeycomb structures. Compos Struct 299:116064. https://doi.org/10.1016/j.compstruct.2022.116064
30. Gorguluarslan R, Gungor U, Yıldız S, Erem E (2019) Lattice-based crash box design by discrete topology optimization for 3D printing. Proceedings to 4th International Congress on 3D Printing (Additive Manufacturing) Technologies and Digital Industry 3D-PTC2019

31. Siebertz K (2017) Statistische Versuchsplanung. Springer Berlin Heidelberg, Berlin, Heidelberg